

Supplementary information

Enabling scalable composite solid electrolyte by cathode-supported scale-up processing

Jiechen Song ^{acd}, Yuxing Xu ^{ad}, Yuncheng Zhou ^{acd}, Rui He ^e, Aijia Wei ^e, Qiangqiang Tan ^{*abcd}

^a State Key Laboratory of Mesoscience and Engineering, Institute of Process Engineering, Chinese Academy of Sciences, Beijing, 100190, China

^b Center of Materials Science and Optoelectronics Engineering, University of Chinese Academy of Sciences, Beijing, 100049, China

^c School of Chemical Engineering, University of Chinese Academy of Sciences, Beijing, 100049, China

^d Hebei Engineering Research Center of Power and Energy Storage Battery Materials, Hebei Technology Innovation Center of Advanced Energy Materials, Hebei Manufacturing Industry Innovation Center of New Energy Materials and Key Equipment, Langfang Technological Service Center of Green Industry, Langfang, 065001, China

^e Institute of Energy Resources, Hebei Academy of Sciences, Hebei, 050081, China

* Corresponding author:

E-mail address: qtan@ipe.ac.cn

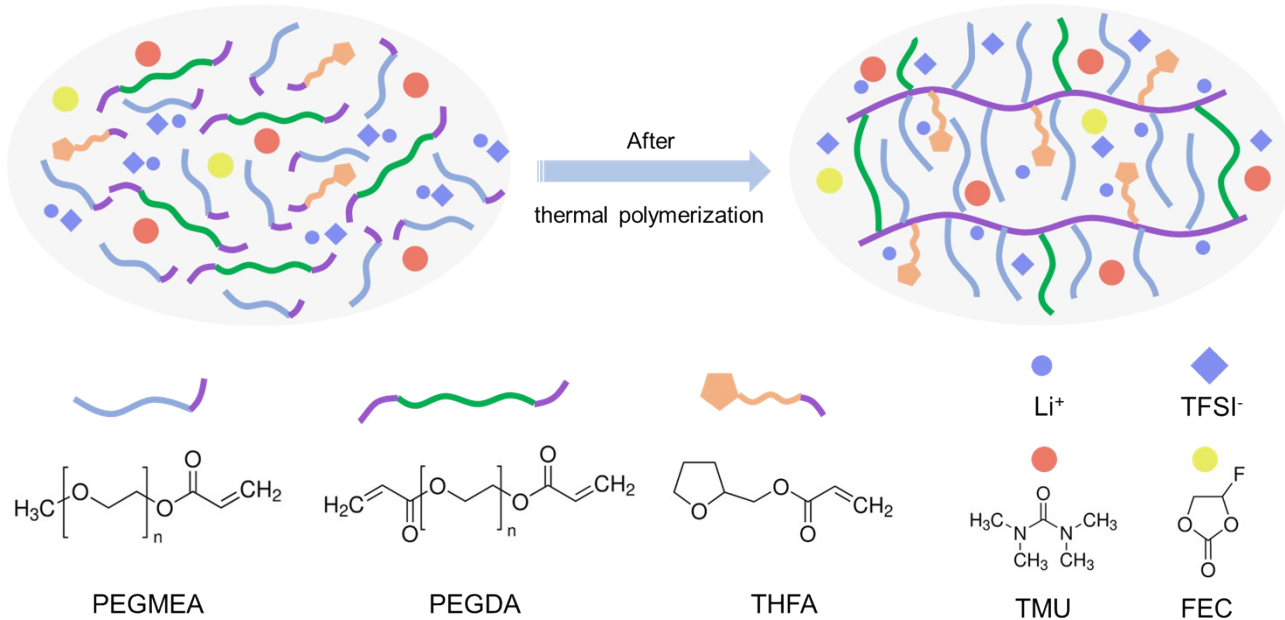


Fig. S1 Schematic diagram of the thermal polymerization procedure and corresponding molecular structures of the PPTTLF electrolyte.

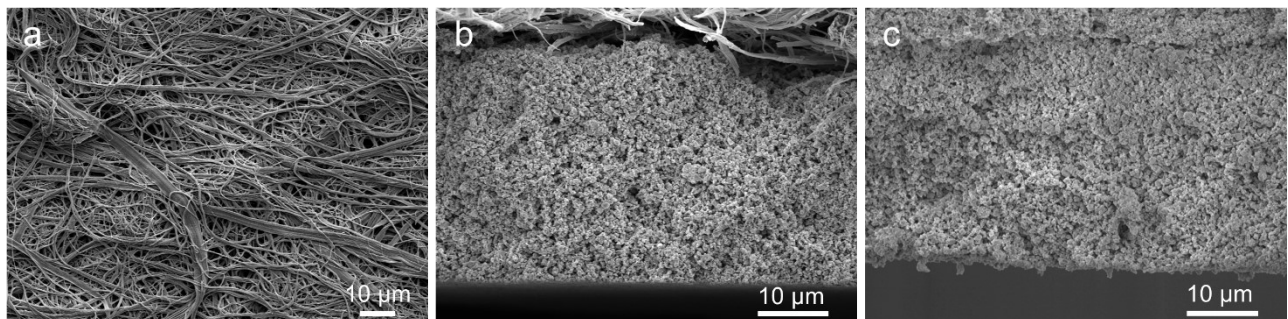


Fig. S2 a) The surface SEM of CM. The cross-sectional SEM of b) CM-supported p-LATP and c) LFP-supported p-LATP at high magnification.

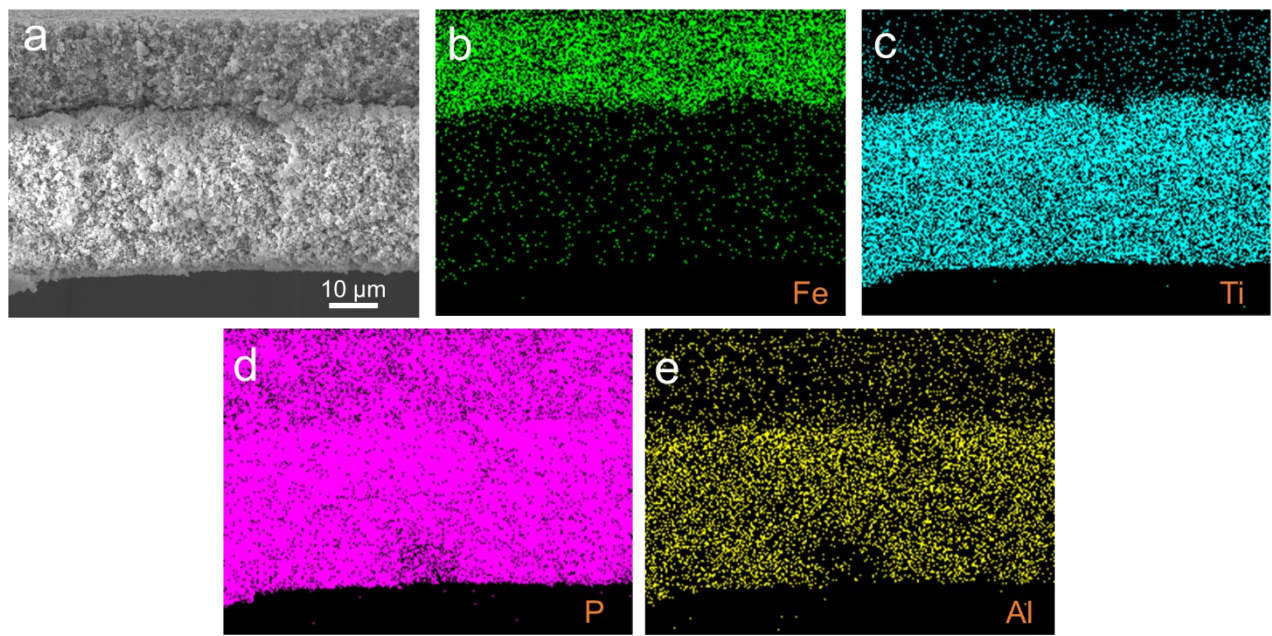


Fig. S3 a) The cross-sectional SEM of the LFP-supported p-LATP. The corresponding EDS element mappings of b) Fe, c) Ti, d) P, and e) Al.

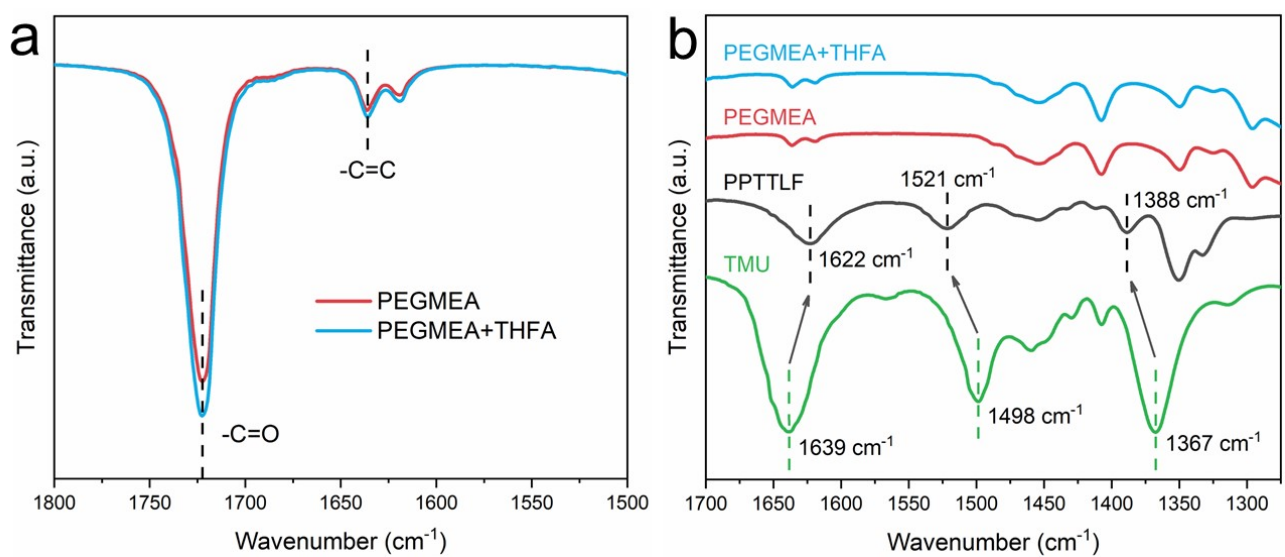


Fig. S4 a) The FTIR spectra of PEGMEA and PEGMEA+THFA. b) The FTIR spectra of TMU, PPTTLF, PEGMEA, and PEGMEA+THFA.

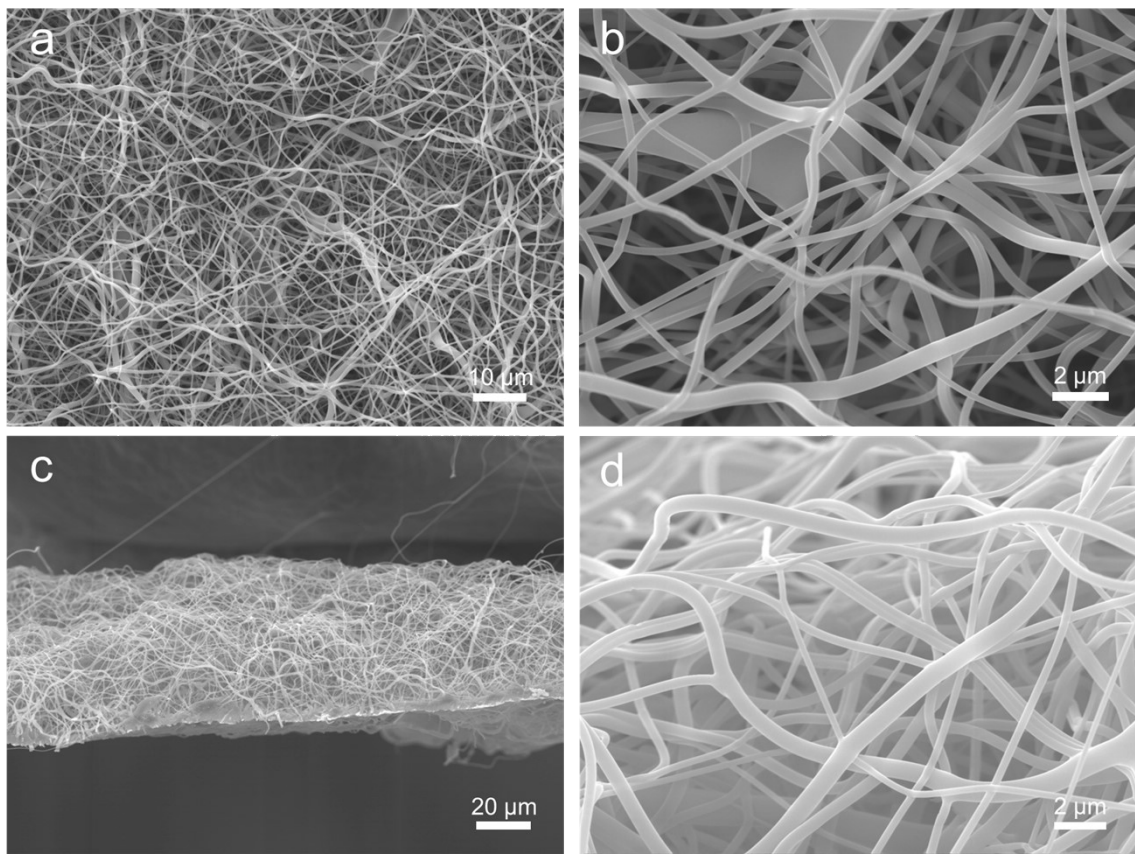


Fig. S5 The surface SEM images of the PI membrane at a) low and b) high magnification. The cross-sectional SEM images of the PI membrane at c) low and d) high magnification.

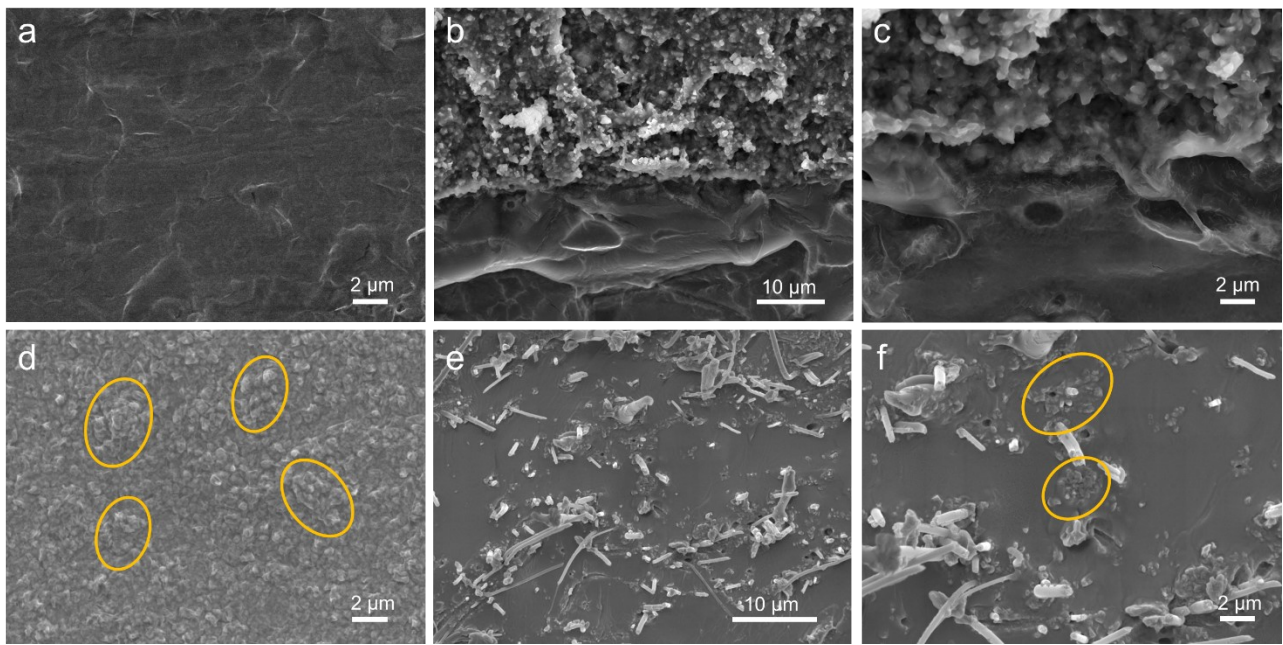


Fig. S6 a) The surface SEM images of PPTTLF@p-LATP CSEs at high magnification. b,c) The cross-sectional SEM images of the interface between PPTTLF@p-LATP CSEs and LFP cathode at high magnification. d) The surface SEM images of PPTTLF-LA@PI CSEs at high magnification. e,f) The cross-sectional SEM images of PPTTLF-LA@PI CSEs at high magnification.

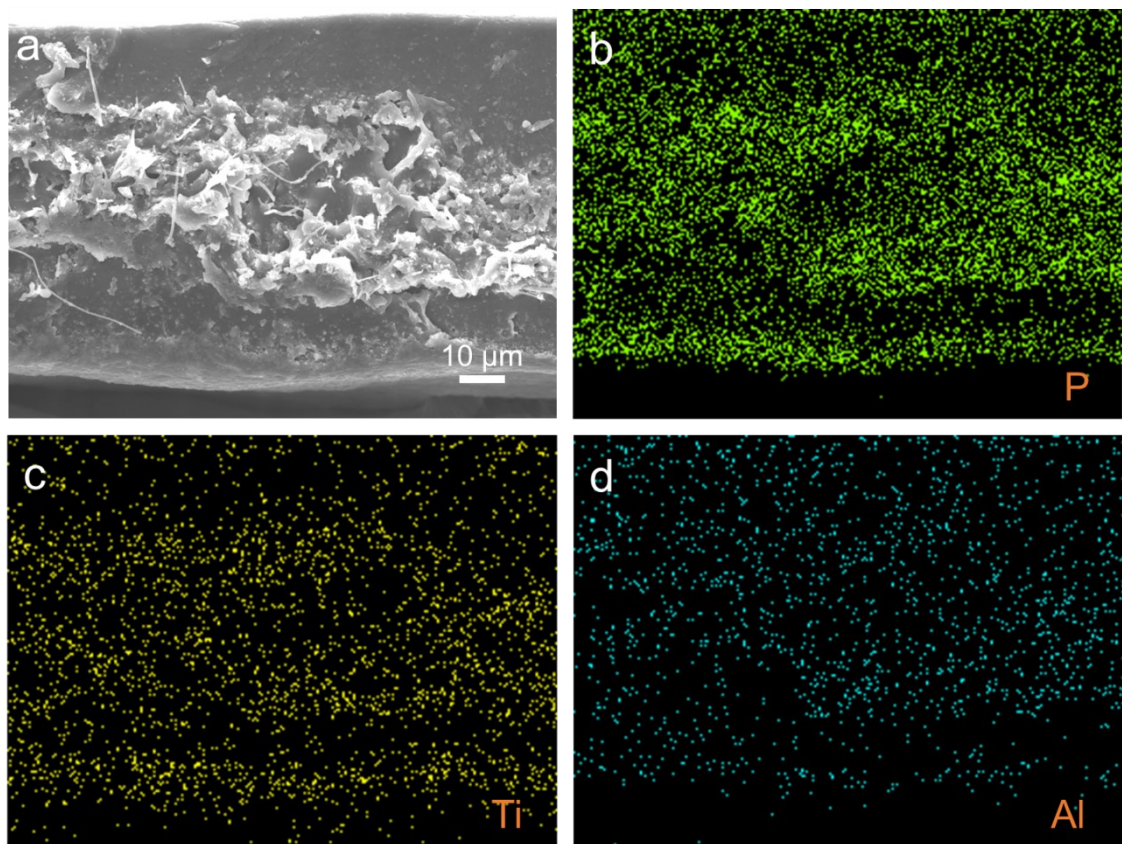


Fig. S7 a) The cross-sectional SEM images of the PPTTLF-LA@PI CSEs. The corresponding EDS element mappings of b) P, c) Ti, and d) Al.

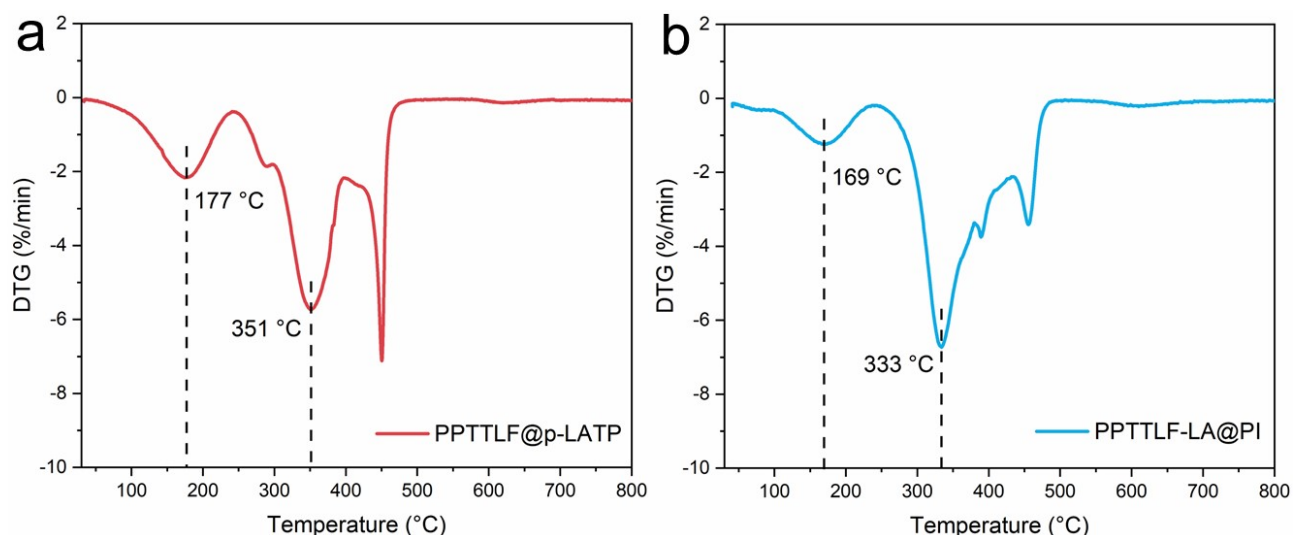


Fig. S8 The DTG curves of a) PPTTLF@p-LATP and b) PPTTLF-LA@PI CSEs.

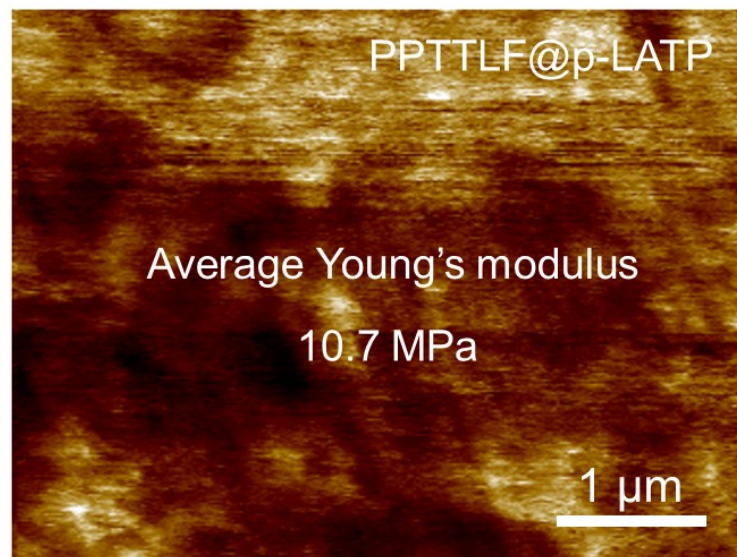


Fig. S9 The AFM measurement for nanoscale mechanical properties of PPTTLF@p-LATP CSEs.

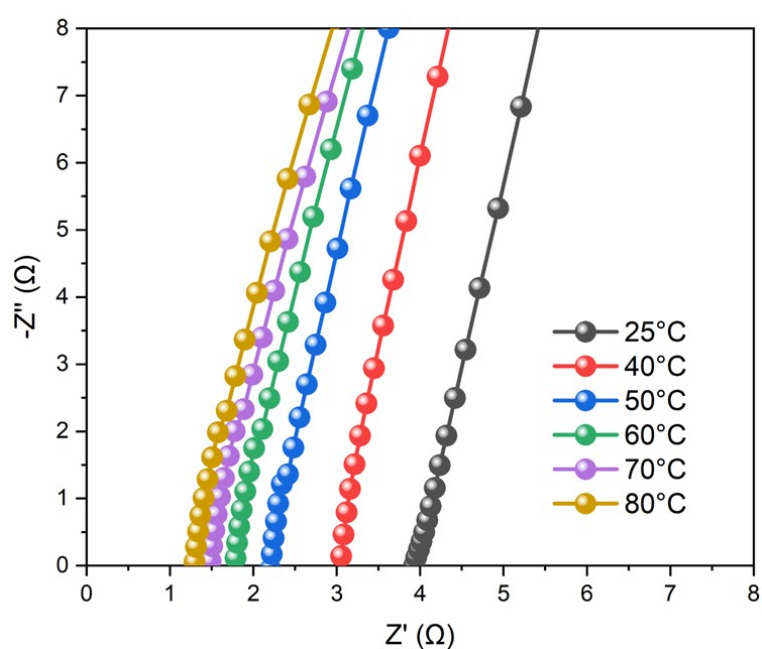


Fig. S10 The Nyquist curve of PPTTLF-LA@PI CSEs at different temperatures.

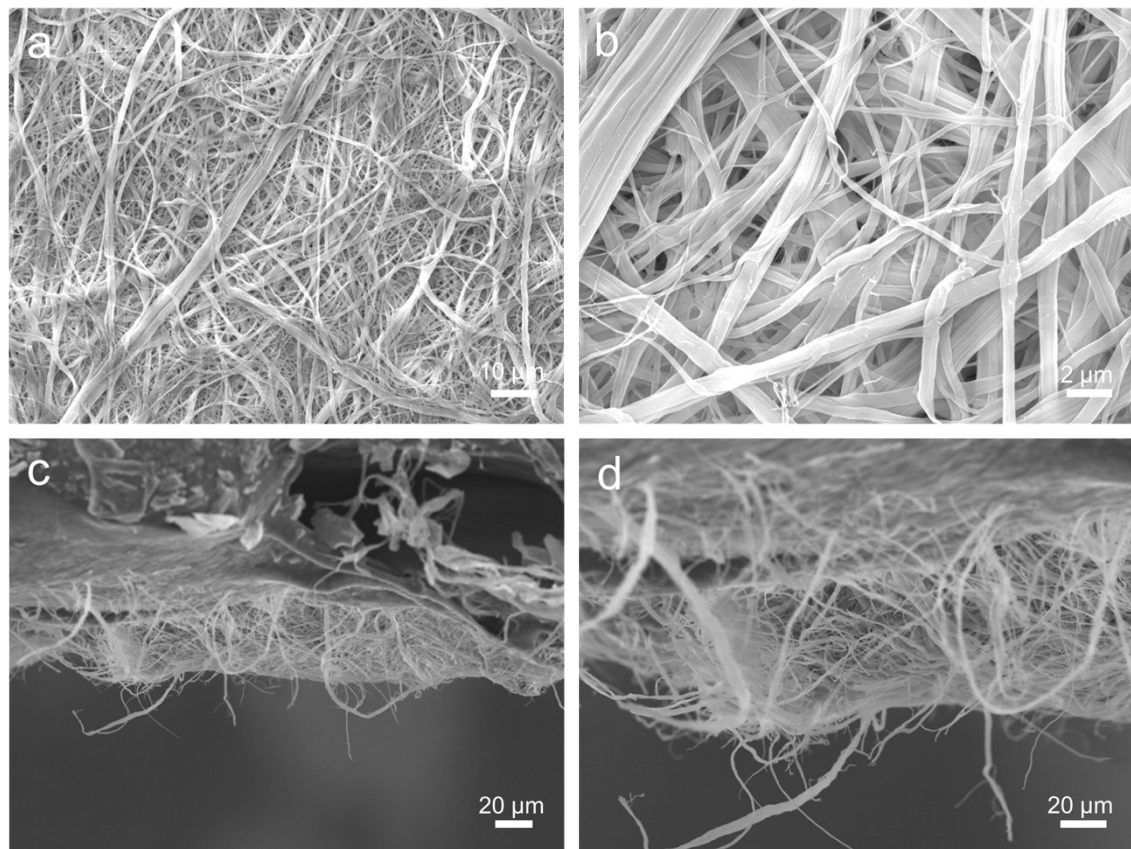


Fig. S11 The surface SEM images of CM at a) low and b) high magnification. The cross-sectional SEM images of CM at c) low and d) high magnification.

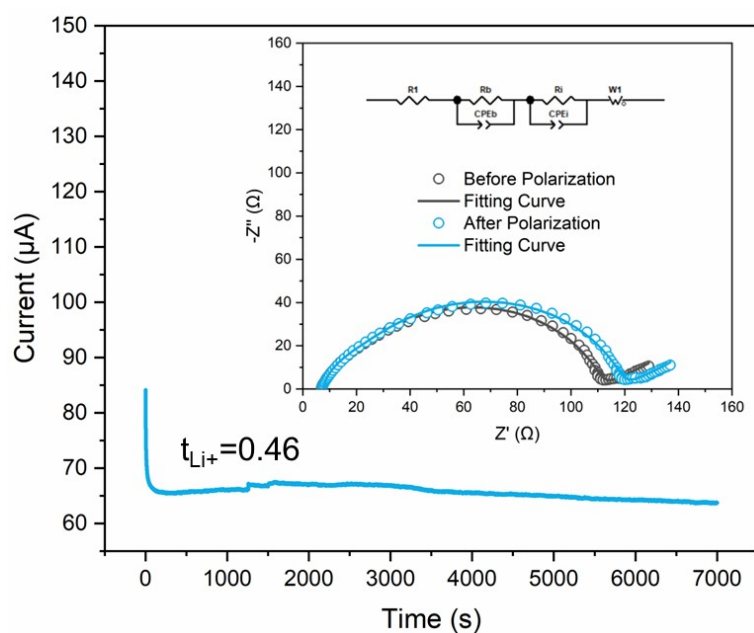


Fig. S12 The i-t curve and the impedance spectra before and after polarization of Li/PPTTLF-LA@PI CSEs/Li cell.

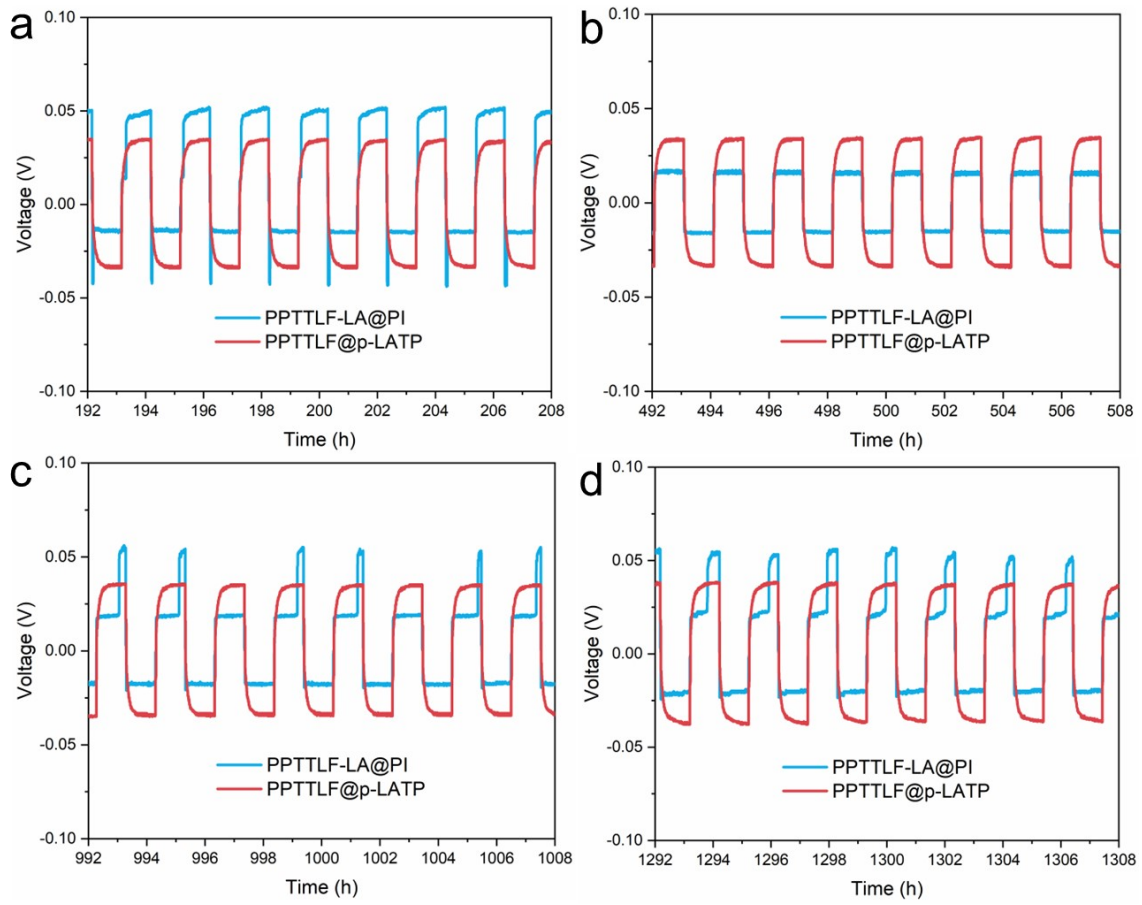


Fig. S13 The enlarged galvanostatic cycling curves of Li/PPTTLF@p-LATP/Li and Li/PPTTLF-LA@PI/Li cells at 0.05 mA cm^{-2} and 0.05 mAh cm^{-2} in the range of a) 192-208 h, b) 492-508 h, c) 992-1008 h, and d) 1292-1308 h.

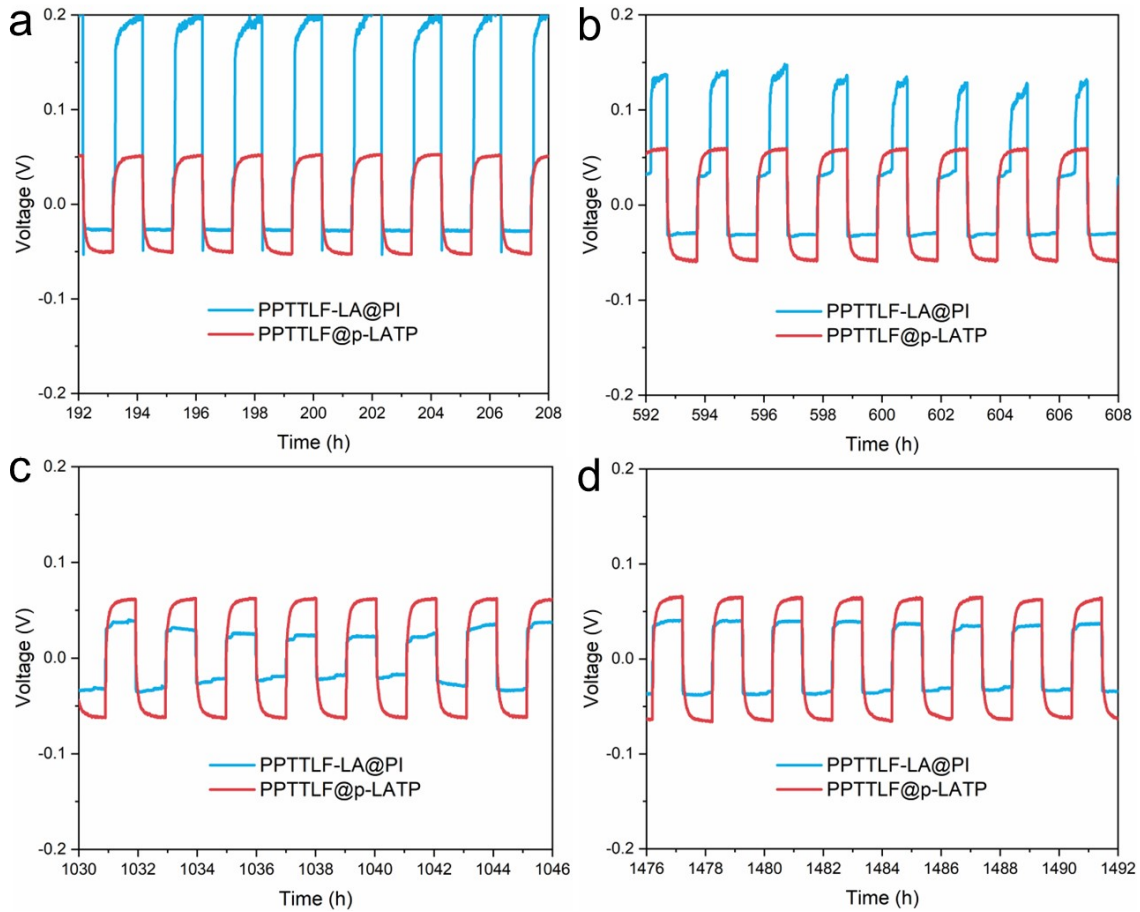


Fig. S14 The enlarged galvanostatic cycling curves of Li/PPTTLE@p-LATP/Li and Li/PPTTLE-LA@PI/Li cells at 0.1 mA cm^{-2} and 0.1 mAh cm^{-2} in the range of a) 192-208 h, b) 592-608 h, c) 1030-1046 h, and d) 1476-1492 h.

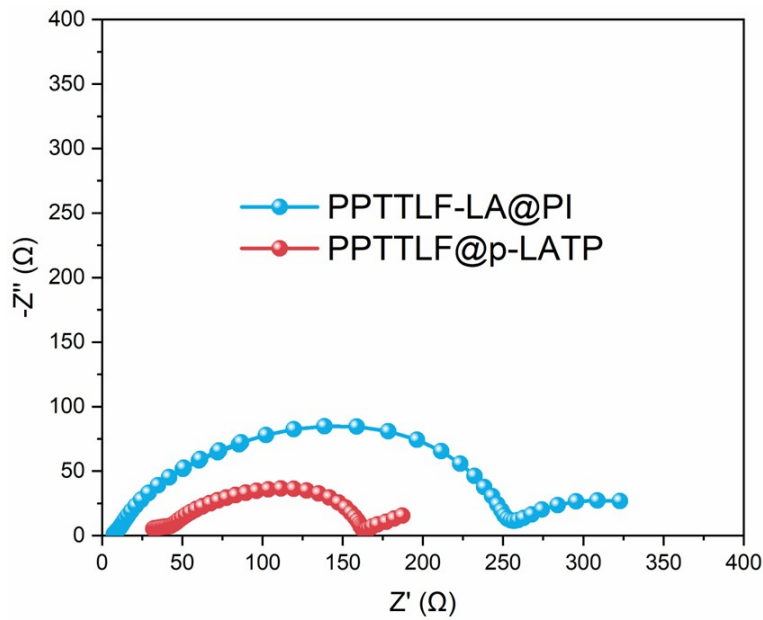


Fig. S15 The impedance curve of Li/PPTTLF@p-LATP/Li and Li/PPTTLF-LA@PI/Li cells after 1645-hour cycling at 0.1 mA cm^{-2} and 0.1 mAh cm^{-2} .

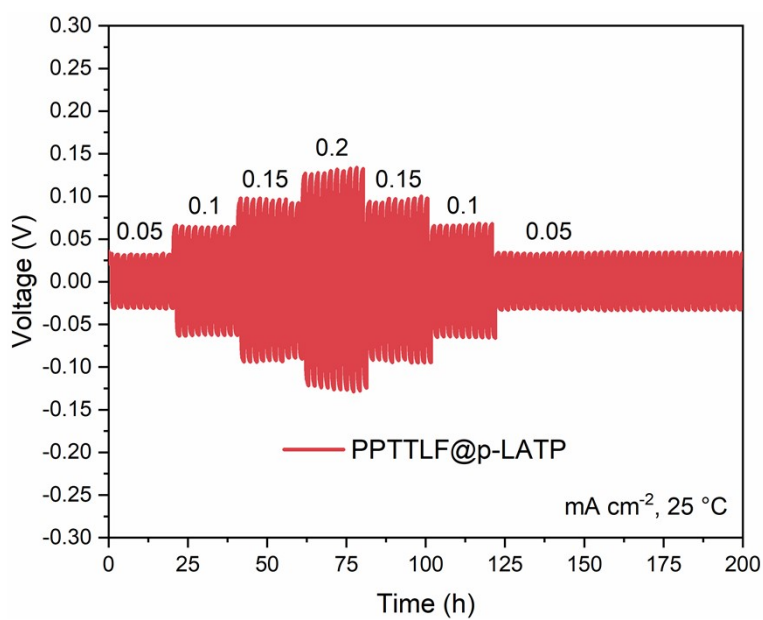


Fig. S16 Galvanostatic cycling curves of Li/Li symmetric cells with PPTTLF@p-LATP CSEs at different current densities. The related areal capacities are 0.05 , 0.1 , 0.15 , and 0.2 mAh cm^{-2} , successively.

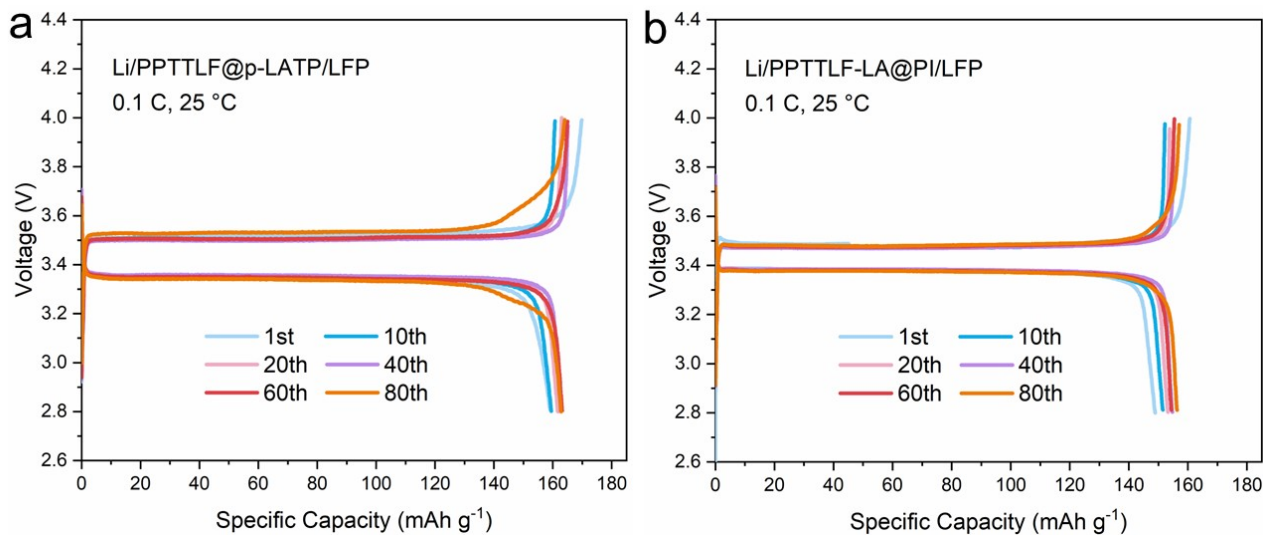


Fig. S17 Galvanostatic charge/discharge curves of Li/LFP full cells with a) PPTTLE@p-LATP and b) PPTTLE-LA@PI CSEs at 0.1 C and 25 °C.

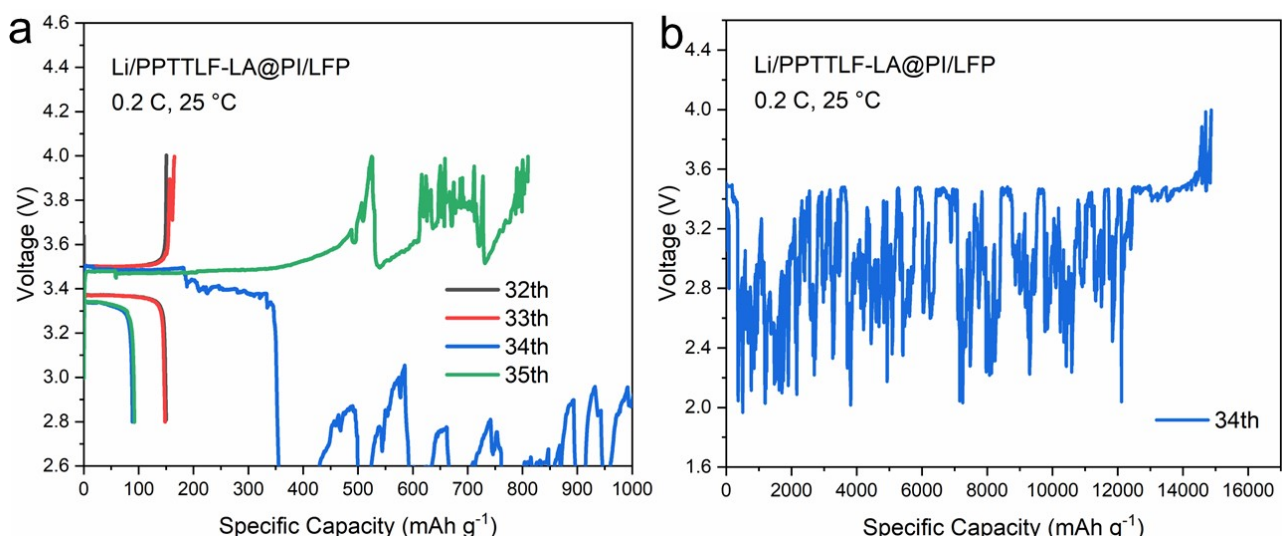


Fig. S18 Galvanostatic charge/discharge curves of Li/LFP full cells with PPTTLE-LA@PI CSEs at 0.2 C and 25 °C a) from the 32th to the 35th cycles and b) at the 34th cycle.

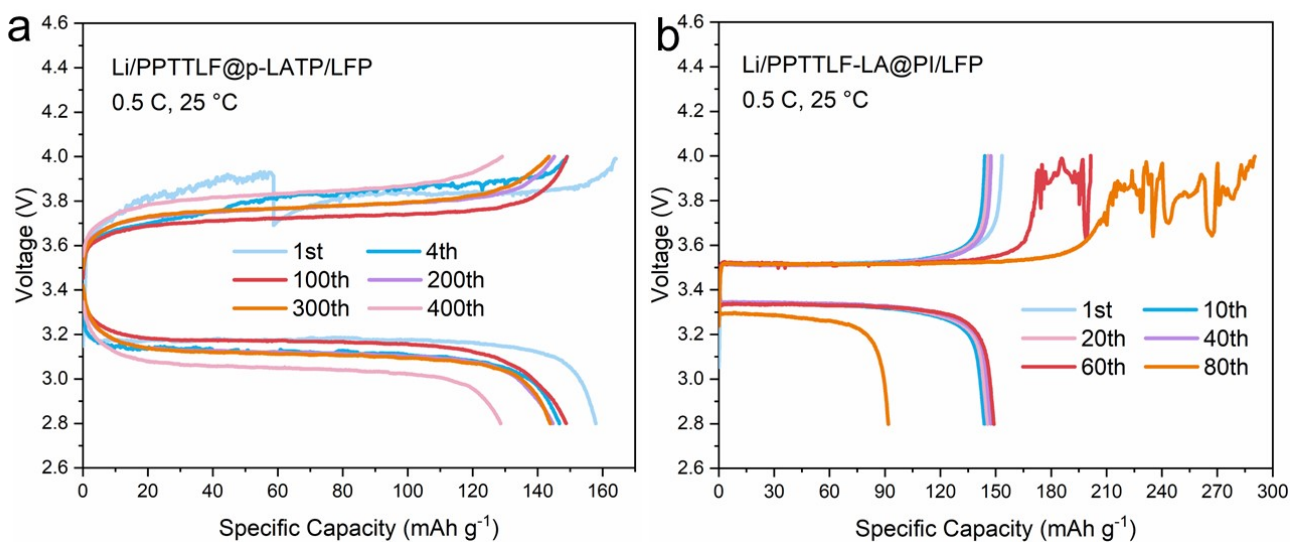


Fig. S19 Galvanostatic charge/discharge curves of Li/LFP full cells with a) PPTTLE@p-LATP and b) PPTTLE-LA@PI CSEs at 0.5 C and 25 °C.

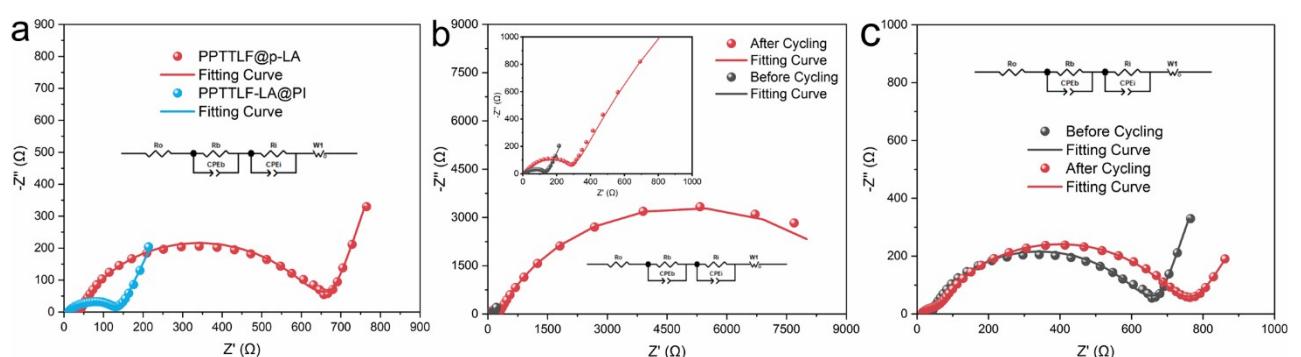


Fig. S20 a) The Nyquist curves of Li/PPTTLE@p-LATP/LFP and Li/PPTTLE-LA@PI/LFP full cells before cycling at 0.5 C. b) The Nyquist curves of the Li/PPTTLE-LA@PI/LFP full cell before cycling and after 89 cycles at 0.5 C. c) The Nyquist curves of the Li/PPTTLE@p-LATP/LFP full cell before cycling and after 145 cycles at 0.5 C.

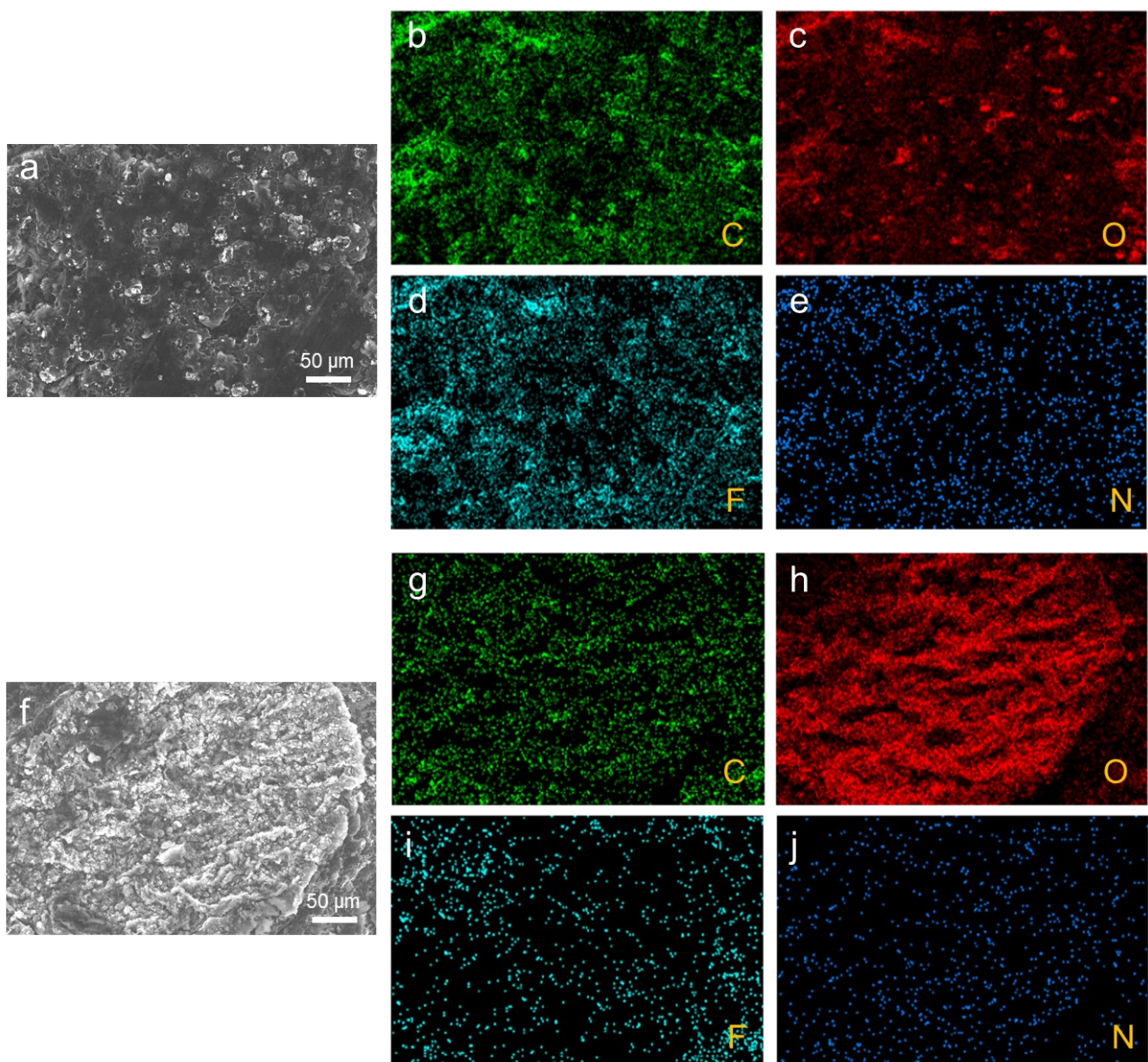


Fig. S21 a) The surface SEM of the Li anode disassembled from the Li/PPTTLF@p-LATP/LFP full cell after 145 cycles at 0.5 C and the corresponding EDS mappings of b) C, c) O, d) F, and e) N elements. f) The surface SEM of the Li anode disassembled from the Li/PPTTLF-LA@PI/LFP full cell after 89 cycles at 0.5 C and the corresponding EDS mappings of g) C, h) O, i) F, and j) N elements.

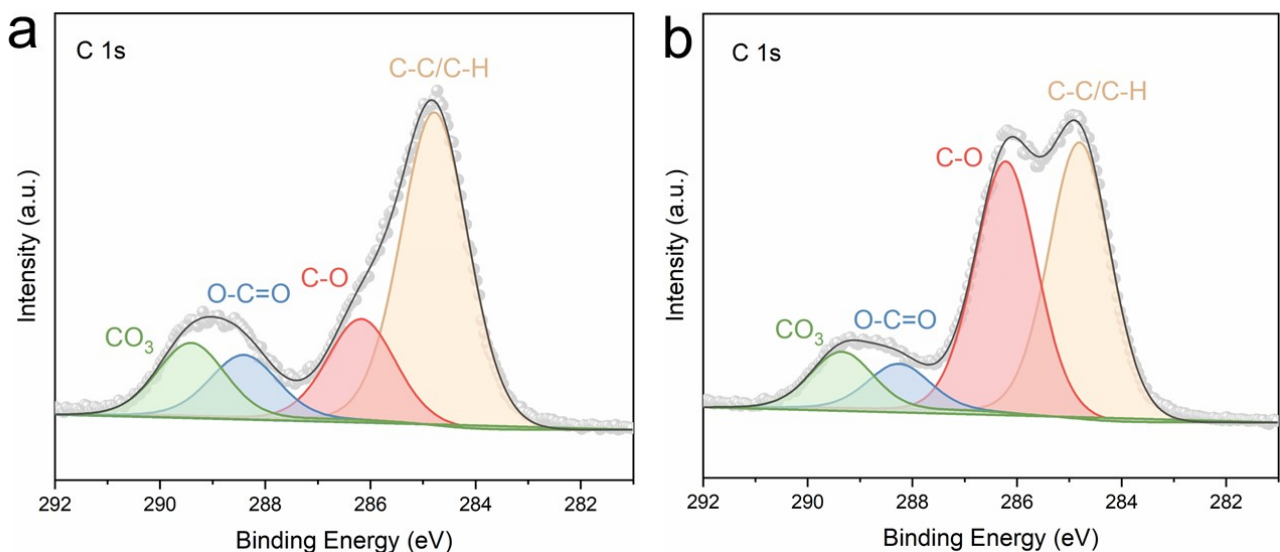


Fig. S22 C 1s XPS spectroscopy of the Li anode surface disassembled from the Li/PPTTLF@p-LATP/LFP and Li/PPTTLF-LA@PI/LFP full cells after 145 cycles and 89 cycles at 0.5 C, respectively.

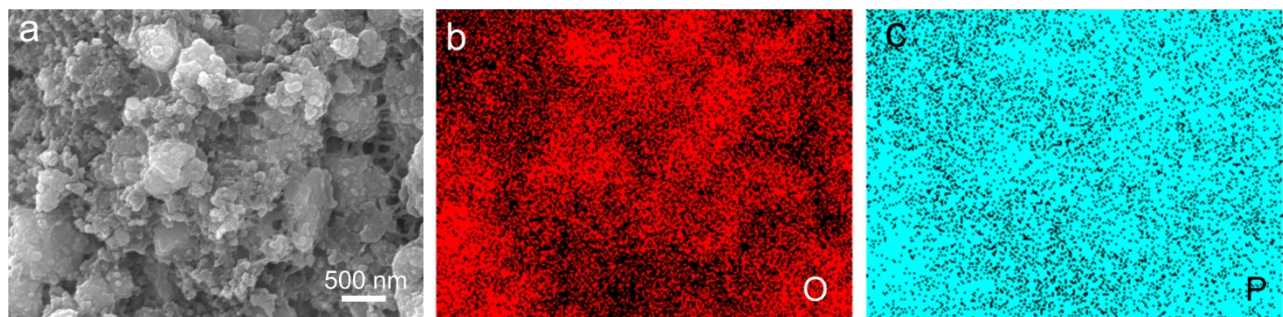


Fig. S23 a) The surface SEM of the LFP cathode disassembled from the Li/PPTTLF@p-LATP/LFP cell after cycling at 0.5 C and corresponding EDS mappings of b) O and c) P elements.

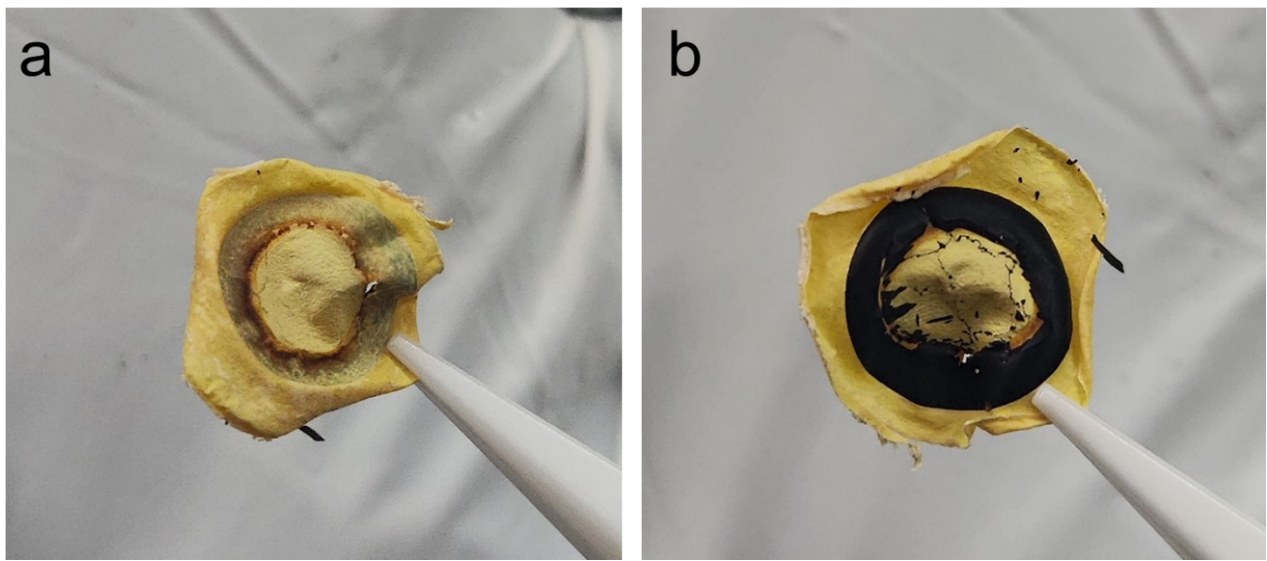


Fig. S24 The LFP with PI membrane disassembled from the Li/PPTTLF-LA@PI/LFP cell after 89 cycles at 0.5 C on the a) PI side and the b) LFP side.

To execute the related characterizations of the cycled LFP cathode and Li anode, the disassembled Li/PPTTLF-LA@PI/LFP full cell is usually immersed into the dimethyl carbonate (DMC) solvent to remove the PPTTLF organic component and separate the cycled electrodes. However, we found that the cycled LFP had been embedded into the PI membrane after removing the PPTTLF organic component (Figure S21a), and it was hard to separate the LFP cathode from the PI membrane. Besides, we found the obvious detached LFP cathode. To observe the detached phenomenon conveniently, we removed the Al foil and exposed the LFP cathode. It can be found that there is an obvious shedding phenomenon in the central region of the cycled LFP cathode (Figure S21b), resulting in the exposed PI membrane on the LFP side. Meanwhile, burnt yellow appears on the edge of the shed LFP cathode, which can be discovered on the PI side in Figure S21a, indicating the inhomogeneous Li^+ deposition and uneven current distribution due to the poor interface stability between the PPTTLF-LA@PI CSEs and LFP cathode.

Table S1 The comparison of the room-temperature ionic conductivities of PPTTLF@p-LATP CSEs with other work.

	Content of CSEs	room-temperature ionic conductivities (mS cm ⁻¹)	Reference
1	PEO+LiTFSI+Ca ₂ Nb ₃ O ₁₀	0.20	¹
2	PEGMA+LiTFSI+LAGP	0.237	²
3	PEGMEA+3D LATP	0.20	³
4	PEO+ PBO+LiTFSI	0.028	⁴
5	PEGDME+PEGDA+P(EO-PO) +LiTFSI+LATP	0.023	⁵
6	PEO+3D LLTO+PEO	0.020	⁶
7	PEO+SN+ZIF-67@CF	0.117	⁷
8	PPTTLF@p-LATP	0.22	This work

Table S2 The ionic conductivities of PPTTLF@p-LATP and PPTTLF-LA@PI CSEs at different temperatures.

Factor	PPTTLF@p-LATP	PPTTLF-LA@PI
$\sigma \times 10^{-4} / \text{S cm}^{-1}$	25°C	2.25
	40°C	3.46
	50°C	5.06
	60°C	7.04
	70°C	9.36
	80°C	11.69
E_a / eV	0.280	0.192

Table S3 The detailed calculation parameters about t_{Li^+} of PPTTLF@p-LATP and PPTTLF-LA@PI CSEs CSEs at room temperature.

Component	$I_0/\mu\text{A}$	$I_{\text{ss}}/\mu\text{A}$	R_0/Ω	R_{ss}/Ω	$\Delta V/\text{mV}$	t_{Li^+}
PPTTLF@p-LATP	3.50	2.32	661.30	641.20	10	0.60
PPTTLF-LA@PI	84.16	63.70	92.05	98.42	10	0.46

Table S4 Performance comparison with Li/PPTTLF@p-LATP/LFP full cells

	Electrolyte compositions	Initial Specific capacity (mAh g^{-1})	Cycle number	Capacity retention	WT* ($^{\circ}\text{C}$)	Current density	Reference
1	PEO+LiTFSI+Ca ₂ Nb ₃ O ₁₀	156.7	440	90%	60	0.5 C	1
2	PEGDE+BDSA+LiTFSI +Py ₁₄ TFSI	143.2	150	90.8%	45	0.5 C	8
3	PEO+PBO+LiSTFSI	158.7	300	73%	60	0.5 C	4
4	BA+PEGDA+LiTFSI+	150.3	250	< 80%	25	0.5 C	9
5	PEG+LiSTFSI+EC	127.5	200	83.2%	28	0.5 C	10
6	PEO+LiTFSI+SN+ZIF67@CF	142.3	150	99%	30	0.2 C	7
7	PEO+p-LLTO	145	50	86.2%	65	0.1 C	6
8	MEA+PEGDA+MPEGA +EMIMTFSI+LiTFSI	146	50	87.1%	25	0.3 C	11
9	EEA+PEGMA+PEGDA +VOD+LiTFSI	138.3	500	93.6%	40	0.5 C	12
		160.1	160	97.9%	25	0.2 C	
10	PPTTLF@p-LATP	146.7	300	96.9%	25	0.5 C	This work
			500	85.8%			

*: working temperature

Table S5 The detailed fitting parameters about impedances of the Li/PPTTLF@p-LATP/LFP and Li/PPTTLF-LA@PI/LFP full cells after cycling at 0.5 C.

Component	R _b of before cycling/Ω	R _i of before cycling /Ω	R _b of after cycling/Ω	R _i of after cycling /Ω
PPTTLF@p-LATP	14.77	570.90	48.63	640.70
PPTTLF-LA@PI	71.93	32.05	299.80	9449.00

References

- 1 L. Yang, B. Li, H. Liu, H. Zhang, Y. Cheng, Q. Li, L. Mai and L. Xu, *Energy Storage Mater.*, 2024, **70**, 103473.
- 2 K. Zhang, F. Wu, X. Wang, S. Weng, X. Yang, H. Zhao, R. Guo, Y. Sun, W. Zhao, T. Song, X. Wang, Y. Bai and C. Wu, *Adv. Energy Mater.*, 2022, **12**, 2200368.
- 3 Y. Yan, J. Ju, S. Dong, Y. Wang, L. Huang, L. Cui, F. Jiang, Q. Wang, Y. Zhang and G. Cui, *Adv. Sci.*, 2021, **8**, 2003887.
- 4 A. Du, H. Lu, S. Liu, S. Chen, Z. Chen, W. Li, J. Song, Q.-H. Yang and C. Yang, *Adv. Energy Mater.*, 2024, **14**, 2400808.
- 5 N. Boaretto, L. Meabe, S. Lindberg, H. Perez-Furundarena, I. Aldalur, E. Lobato, F. Bonilla, I. Combarro, A. Gutiérrez-Pardo, A. Kvasha, M. Lechartier, R. Vincent, J. Cognard, S. Genies, L. Daniel and M. Martinez-Ibañez, *Adv. Funct. Mater.*, 2024, DOI: <https://doi.org/10.1002/adfm.202404564>, 2404564.
- 6 Z. Jiang, S. Wang, X. Chen, W. Yang, X. Yao, X. Hu, Q. Han and H. Wang, *Adv. Mater.*, 2020, **32**, 1906221.
- 7 X. Song, K. Ma, J. Wang, H. Wang, H. Xie, Z. Zheng and J. Zhang, *ACS Nano*, 2024, **18**, 12311-12324.
- 8 X. Wang, S. Huang, X. Sun, Y. Chen, J. Zheng, S. Zhang and S. Li, *Energy Storage Mater.*, 2024, **70**, 103526.
- 9 S. Wang, Q. Lv, Y. Jing, B. Wang, D. Wang, H. Liu and S. Dou, *Energy Storage Mater.*, 2024, **69**, 103390.
- 10 T. Guan, Z. Rong, F. Cheng, W. Zhang and J. Chen, *ACS Appl. Energy Mater.*, 2020, **3**, 12532-12539.
- 11 S. Qin, Y. Cao, J. Zhang, Y. Ren, C. Sun, S. Zhang, L. Zhang, W. Hu, M. Yu and H. Yang, *Carbon Energy*, 2023, **5**, e316.
- 12 S. Qin, Y. Yu, J. Zhang, Y. Ren, C. Sun, S. Zhang, L. Zhang, W. Hu, H. Yang and D. Yang, *Adv. Energy Mater.*, 2023, **13**, 2301470.